

Successive magnetic phase transitions of a Co vermiculite intercalation compound: An Ising-like Heisenberg antiferromagnet on a triangular lattice

Itsuko S. Suzuki* and Masatsugu Suzuki

Department of Physics, State University of New York at Binghamton, Binghamton, New York 13902-6016

N. Wada

Department of Mechanical Engineering, Faculty of Engineering, Toyo University, 2100 Kujirai, Kawagoe City, Saitama, 350-8585 Japan

(Received 24 August 2001; published 26 March 2002)

A Co vermiculite intercalation compound (VIC) magnetically behaves as an Ising-like Heisenberg antiferromagnet on a triangular lattice. Magnetic properties of a Co VIC have been studied using superconducting quantum interference device (SQUID) dc magnetization and SQUID ac magnetic-susceptibility measurements. This compound undergoes magnetic phase transitions at T_{N1} ($=16.3$ K) and T_{N2} ($=10.7$ K), and shows magnetic anomalies at T_{p1} ($=7.7$ K), T_{p2} ($=5.9$ K), and T_{p3} (≈ 3 K). The c -axis spin order and the in-plane spin order occur at T_{N1} and T_{N2} , respectively. The magnetic phase diagram for $H\parallel c$ consists of four phases whose boundaries meet at a multicritical point ($T_m \approx 12$ K, $H_m \approx 25$ kOe). The freedom of rotation around an axis perpendicular to the spin plane where three sublattice-magnetization vectors lie could be frozen out below T_{p1} or T_{p2} . A superparamagnetic behavior of Arrhenius type is observed around T_{p3} .

DOI: 10.1103/PhysRevB.65.134438

PACS number(s): 75.50.Lk, 75.40.Gb, 75.40.Cx, 75.70.Cn

I. INTRODUCTION

In the last two decades, the spin frustration in Ising antiferromagnets on a triangular lattice has been studied experimentally¹⁻⁴ and theoretically.⁵⁻⁷ The Ising model with antiferromagnetic nearest-neighbor (NN) interactions is the simplest spin system, which is totally frustrated. It exhibits no long-range spin order at a finite temperature because of the macroscopic degeneracy of the ground state. An additional interaction such as the ferromagnetic next-nearest-neighbor (NNN) interaction or interplanar interaction, which removes the degeneracy, may assist the system to order. The ordering process shows characteristic features: successive transitions at Néel temperatures T_{N1} and T_{N2} . The intermediate phase between T_{N1} and T_{N2} is a partially disordered (PD, denoted by type I for convenience) phase, where two of three sublattices are oppositely magnetized and the other one remains paramagnetic. The low-temperature phase below T_{N2} is a ferrimagnetic (FR, type II) phase where one of the three sublattices magnetizes oppositely to the other two. CsCoCl₃ (Refs. 1-4) and CuFeO₂ (Refs. 8-10) have been proven to be typical examples for a three-dimensional (3D) realization of an Ising antiferromagnet on the triangular lattice: $T_{N1}=21$ K and $T_{N2}=9$ K for CsCoCl₃ and $T_{N1}=14.0$ K and $T_{N2}=11.0$ K for CuFeO₂.

The phase transition of the Ising-like Heisenberg antiferromagnet on the triangular lattice (IHAFT) has been studied by Miyashita and Kawamura,¹¹ and Miyashita.^{12,13} The spin Hamiltonian of this system is described by

$$H = -2J \sum_{\langle i,j \rangle} [S_i^x S_j^x + S_i^y S_j^y + \alpha S_i^z S_j^z], \quad (1)$$

where $J < 0$ and $\alpha > 1$, $\langle i,j \rangle$ means NN pairs, and $\alpha = 1$ for the Heisenberg model and $\alpha = \infty$ for the Ising model. No NNN ferromagnetic interaction is included in this Hamiltonian.

Only the xy interaction is added to the Ising interaction. A Monte Carlo analysis of the IHAFT predicts successive phase transitions at T_{N1} and T_{N2} without long-range orders. The value of T_{N1} increases with increasing α , while the value of T_{N2} decreases. In the intermediate phase between T_{N1} and T_{N2} , there is no uniform magnetization along the z axis. The spin configuration corresponds to that of either the PD phase or the FR phase with the total of three sublattice magnetizations equal to zero. Below T_{N2} the xy components start to order. The uniform susceptibilities χ_{zz} , χ_{xx} , and χ_{yy} diverge. The divergence of χ_{xx} and χ_{yy} may be attributed to the effect of a nontrivial degeneracy (NTD) of the ground-state spin configuration. Namely, infinite numbers of obliquely distorted 120° structures (type III) give the same ground-state energy. Due to this NTD the ground state can have the xy component of total magnetization (M_x and M_y).

In three dimensions, systems have long-range orders in contrast to two dimensions. Thus, the spin configuration can be specified. The corresponding 3D lattice is a layered antiferromagnet on a triangular lattice (AFT), called an Ising-like Heisenberg layered AFT (IHLAFT). The spin Hamiltonian of this system is described by

$$H = -2J \sum_{\langle i,j \rangle} [S_i^x S_j^x + S_i^y S_j^y + \alpha S_i^z S_j^z] - 2J' \sum_{\langle i,k \rangle} \mathbf{S}_i \cdot \mathbf{S}_k, \quad (2)$$

where $\langle i,k \rangle$ means NN pairs between layers, and the interplanar coupling is isotropic. The NTD in the ground state persists just as in the 2D case. According to Monte Carlo studies of the IHLAFT by Watarai and Miyashita,^{14,15} this system exhibits similar transitions as in the case of an IHAFT but with a definite long-range order. At T_{N1} the system undergoes a change from the paramagnetic (PM) phase to the FR phase (type II). The order of the xy components

appears below T_{N2} , resulting in the obliquely distorted 120° structure (type III) characterized by two angles φ and θ . Here φ is the angle between the z axis and the direction of sublattice magnetization A , and 2θ is the angle between the directions of sublattice magnetizations B and C , where $\cos \theta = \alpha/(\alpha+1)$. The ground-state energy of the type-III spin structures is independent of φ .

A Co vermiculite intercalation compound (VIC) provides a candidate for the IHLAFT. This system is one of magnetic VIC's (Refs. 16–18) with well-characterized expanding layered silicates. The Co VIC is frequently in the two-water-layer hydration state (2-WLHS) under normal ambient conditions, where Co^{2+} ions are sandwiched between upper and lower water layers in the interlamellar space. In this paper we have undertaken an extensive study of the magnetic properties of a Co VIC with a 2-WLHS using superconducting quantum interference device (SQUID) dc magnetization and SQUID ac magnetic susceptibility. We show that this compound undergoes at least two magnetic phase transitions at T_{N1} ($=16.3$ K) and T_{N2} ($=10.7$ K). These phase transitions are discussed in association with the two transitions of the IHLAFT model developed by Watarai and Miyashita.^{14,15} The magnetic phase diagram (H - T) is determined and discussed, where H is an external magnetic field and T is a temperature. The irreversible effect of susceptibility, which shows steplike changes around T_{N1} and T_{N2} , is discussed in terms of the random-field effect. A superparamagnetic behavior is observed at lower temperatures. The temperature dependence of a spin relaxation time is discussed in terms of the Arrhenius law.

II. EXPERIMENT

Single crystals of natural vermiculite normally contain Mg^{2+} ions in the interlamellar space, forming a Mg VIC. Samples used in the present work were prepared from natural vermiculites obtained from Llano, Texas. They were immersed in one normal aqueous solution of CoCl_2 at 60°C. Mg^{2+} ions can be replaced by Co^{2+} ions, forming a Co VIC. The unit-cell stoichiometry of a Co VIC with the 2-WLHS is given by $X\text{Co}_u(\text{H}_2\text{O})_{6,10}$, where $X=(\text{Si}_{5.72}\text{Al}_{2.28})$ ($\text{Mg}_{5.88}\text{Al}_{0.10}\text{Fe}_{u'}\text{Ti}_{0.02}$) $\text{O}_{20}(\text{OH})_4$, u' ($=0.03$) is the number of Fe ions in the octahedral sheet, and u ($=0.76 \pm 0.08$) is the number of Co^{2+} ions in the interlamellar space.¹⁶ The total molar mass of the unit-cell stoichiometry for a Co VIC is estimated as $M_{\text{Co}}=911$ g. It was confirmed from a (00L) x-ray diffraction at 300 K that our sample had a well-defined c -axis stacking structure with the c -axis repeat distance d ($=14.377 \pm 0.004$ Å) for the 2-WLHS.

The dc magnetization and ac magnetic susceptibility of the Co VIC were measured using a SQUID magnetometer (Quantum Design, MPMS XL-5) with an ultralow-field capability option. The details of the measurements were described in a previous paper.¹⁸ The magnetic field was applied to either the c axis or any direction perpendicular to the c axis. For convenience, hereafter we use “ a axis” for any direction in the c plane, since there may be no appreciable magnetic anisotropy in the c plane.

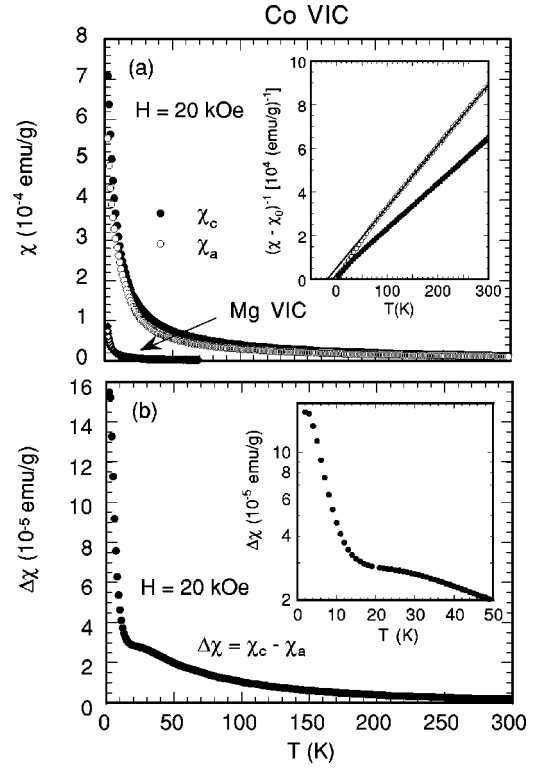


FIG. 1. (a) T dependence of dc magnetic susceptibility χ_c (closed circles) and χ_a (open circles) for a Co VIC with a 2-WLHS, and χ_c (closed diamonds) and χ_a (open diamonds) for a Mg VIC with a 2-WLHS (natural vermiculite). $H=20$ kOe. The inset shows the reciprocal susceptibility $(\chi - \chi_0)^{-1}$ as a function of T for a Co VIC. The solid lines denote the least-squares fits of the data to Eq. (3) with parameters given in the text. (b) T dependence of $\Delta\chi$ ($=\chi_c - \chi_a$) for a Co VIC at $H=20$ kOe.

III. RESULTS

A. dc magnetic susceptibility

Figure 1 shows the T dependence of dc magnetic susceptibility for a Co VIC with a 2-WLHS in the presence of H ($=20$ kOe) along the c axis and a axis. The magnetic susceptibility increases with decreasing T , obeying the Curie-Weiss law. The susceptibility along the c axis (χ_c) is larger than that along the a axis (χ_a). The least-squares fit of the data for $150 \leq T \leq 298$ K to the Curie-Weiss form

$$\chi_i = \chi_i^0 + \frac{C_i}{T - \Theta_i} \quad (3)$$

($i=c,a$) yields the parameters $\chi_c^0 = (-2.52 \pm 0.09) \times 10^{-6}$ emu/g, $C_c = (4.65 \pm 0.04) \times 10^{-3}$ emu K/g, and $\Theta_c = -8.43 \pm 0.96$ K for the c axis, and $\chi_a^0 = (-5.16 \pm 0.82) \times 10^{-7}$ emu/g, $C_a = (3.55 \pm 0.05) \times 10^{-3}$ emu K/g, and $\Theta_a = -17.9 \pm 1.2$ K for the a axis. Assuming $u=0.76$ and $u' \approx 0$, the effective magnetic moment $P_{eff}(\text{Co}^{2+})$ can be estimated as $6.68 \pm 0.03 \mu_B$ for the c axis and $5.83 \pm 0.03 \mu_B$ for the a axis, which are comparable with those for Co^{2+} ions for CsCoCl_3 : $6.14 \mu_B$ for the c axis and $5.54 \mu_B$ for the a axis.¹⁹ When we use a fictitious spin $S=1/2$ for the lowest Kramers doublet instead of $S=3/2$ (see Sec. IV E),

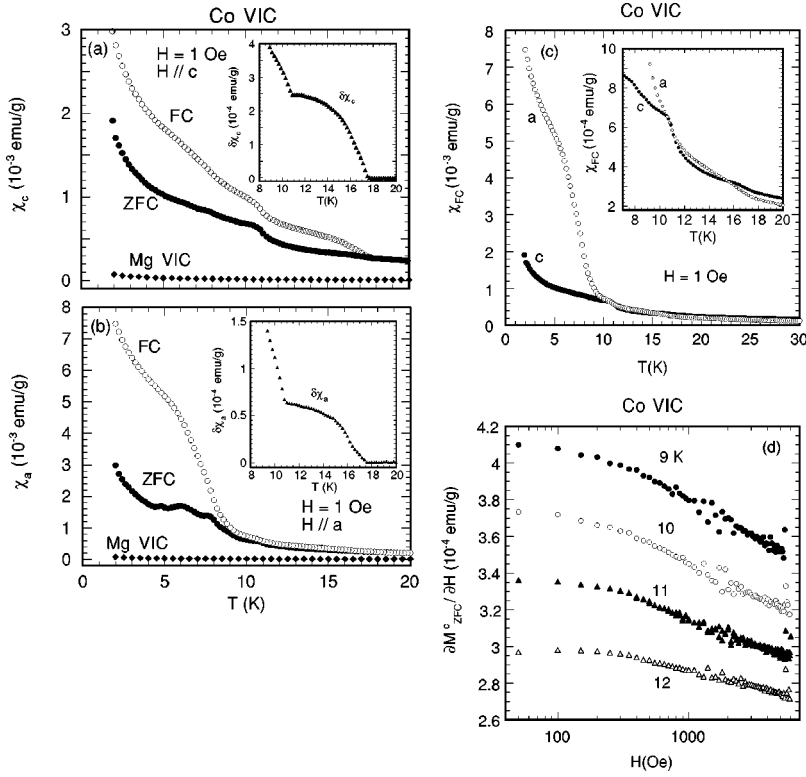


FIG. 2. (a) and (b) T dependence of χ_{FC} (open circles) and χ_{ZFC} (closed circles) for a Co VIC and χ_{FC} (closed diamonds) for a Mg VIC. $H=1$ Oe. (a) $H \parallel c$. (b) $H \parallel a$. The insets of (a) and (b) show the T dependence of the difference $\delta\chi_i (= \chi_{FC}^i - \chi_{ZFC}^i)$ for $i=c$ and a . (c) T dependence of χ_{FC}^c and χ_{ZFC}^c at $H=1$ Oe. The detail is shown in the inset. (d) H dependence of $\partial M_{ZFC}^c / \partial H$ at $T=9-12$ K, where each measurement was made after the sample was cooled at $H=0$ from 298 K to T .

the Landé g factor is estimated as $g_c = 7.71$, which is close to that ($g_c = 7.32$) for 1% Co^{2+} ions in CsMgCl_3 determined from electron-spin resonance.¹⁹ The negative value of Θ indicates that the NN intraplanar exchange interaction between Co^{2+} spins is antiferromagnetic. In Fig. 1(b) we show the T dependence of the difference $\Delta\chi (= \chi_c - \chi_a)$ at $H=20$ kOe. The difference $\Delta\chi$ is always positive for any T .

Figures 2(a) and 2(b) show the T dependence of field cooled (FC) susceptibility χ_{FC}^i and zero-field cooled (ZFC) susceptibility χ_{ZFC}^i for $i=c$ and a , where $H=1$ Oe. The susceptibility χ_{ZFC}^a has small peaks around 4.8, 6.0, and 7.8 K, while χ_{FC}^a has an inflection point around 5.2 K. In the insets of Figs. 2(a) and 2(b) we show the T dependence of the irreversibility of susceptibility which is defined by $\delta\chi_i (= \chi_{FC}^i - \chi_{ZFC}^i)$. We find that both $\delta\chi_c$ and $\delta\chi_a$ exhibit two steplike increases at 17.5 and 10.7 K with decreasing T , reflecting the disordered nature of this system.

For comparison, in Fig. 2(c) we show the T dependence of χ_{FC}^c and χ_{ZFC}^c at $H=1$ Oe. The susceptibility χ_{ZFC}^c is larger than χ_{FC}^c below 10.7 K, suggesting that the low temperature phase below T_{N2} ($=10.7$ K) has an antiferromagnetic character with the easy spin direction along the c axis. The susceptibility χ_{FC}^c is larger than χ_{ZFC}^c above 15.6 K, which is consistent with the positive sign of $\Delta\chi$ at $H=20$ kOe.

We have measured the H dependence of ZFC magnetization along the c axis (M_{ZFC}^c) around T_{N2} . The magnetization M_{ZFC}^c increases with increasing H for $H \leq 6$ kOe. In Fig. 2(d) we show the H dependence of $\partial M_{ZFC}^c / \partial H$ at $T=9-12$ K. It exhibits a broad peak around $H=0.1$ kOe at $T=12$ K.

B. ac magnetic susceptibility

Figures 3(a)–3(d) show the T dependence of χ'_{cc} and χ''_{cc} for a Co VIC at various f , where $h=2$ Oe. The dispersion χ'_{cc} shows a cusp at T_{N2} , below which it is dependent on f . It has an inflection point around T_{N1} ($=16.3$ K), which is almost independent of f . In contrast, χ''_{cc} exhibits at least four peaks at characteristic temperatures T_{N1} , T_{p1} ($=7.7$ K), T_{p2} ($=5.9$ K), and T_{p3} (≈ 3 K) at $f=0.1$ Hz. The peak temperatures T_{N1} , T_{p1} , and T_{p2} are almost independent of f , while the peak temperature T_{p3} increases with increasing f . The f dependence of T_{p3} will be discussed in Sec. IV C. The absorption χ''_{cc} reduces to zero around T_{N2} .

Figures 4(a) and 4(b) show the T dependence of χ'_{aa} and χ''_{aa} for a Co VIC at various f , where $h=2$ Oe. The dispersion χ'_{aa} shows shoulders around T_{N2} and T_{p1} and a small peak at T_{p2} , while χ''_{aa} shows peaks at T_{p1} and T_{p2} . No anomaly is observed around T_{N1} for both χ'_{aa} and χ''_{aa} . The magnitudes of χ'_{aa} and χ''_{aa} are much larger than those of χ'_{cc} and χ''_{cc} , respectively, at the same T below T_{N2} .

Figures 5(a) and 5(b) show the T dependence of χ'_{cc} for a Co VIC at various H along the c axis, where $h=2$ Oe and $f=100$ Hz. A shoulder around T_{N2} at $H=0$ disappears above 700 Oe, while a broad peak appears at 6.9 K above 15 kOe, shifting to the high- T side with increasing H . For more details the same measurement was taken one year later after the measurement of Fig. 5 was taken. Figure 6 shows the T dependence of χ'_{cc} at various H thus obtained. The peak temperature of χ'_{cc} in Fig. 6 is higher than that in Fig. 5(b) at the same H , partly because of a possible change in the quality of the sample such as the water hydration state. In spite of this,

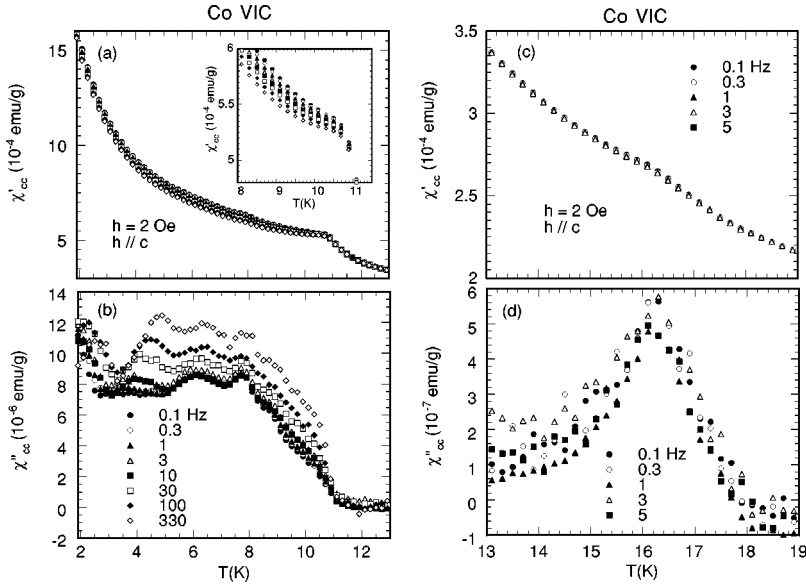


FIG. 3. T dependence of (a) χ'_{cc} and (b) χ''_{cc} for a Co VIC at various f ($1.9 \leq T \leq 13$ K). $h = 2$ Oe. $h \parallel c$. $H = 0$. The detail of χ'_{cc} vs T around T_{N2} is shown in the inset. T dependence of (c) χ'_{cc} and (d) χ''_{cc} for a Co VIC at various f ($13 \leq T \leq 19$ K).

we use the peak temperatures of χ'_{cc} in Fig. 6 for the discussion of the magnetic phase diagram (Sec. IV B). Figure 7 shows the T dependence of χ''_{cc} for a Co VIC at various H along the c axis. Both peaks at T_{p1} and T_{p2} are sensitive to H and disappear above 25 Oe. Although no peak is observed around T_{N2} at $H = 0$, a field-induced peak appears at 11.2 K just above T_{N2} for $0.3 \text{ kOe} \leq H \leq 5 \text{ kOe}$. This peak slightly shifts to the high- T side with increasing H . Above 10 kOe

χ''_{cc} increases with decreasing T . The magnitude of χ''_{cc} drastically increases with increasing H at the same T . In contrast, the peak at T_{N1} at $H = 0$ slightly decreases with increasing H and disappears above 150 Oe. Figure 8(a) shows the T dependence of χ'_{aa} for a Co VIC at various H along the a axis, where $h = 2$ Oe and $f = 100$ Hz. The shoulders at T_{p1} and T_{p2} are very sensitive to H and disappear above 100 Oe. A small shoulder around T_{N2} at $H = 0$ disappears above 100 Oe. Figure 8(b) shows the T dependence of χ''_{aa} for a Co VIC

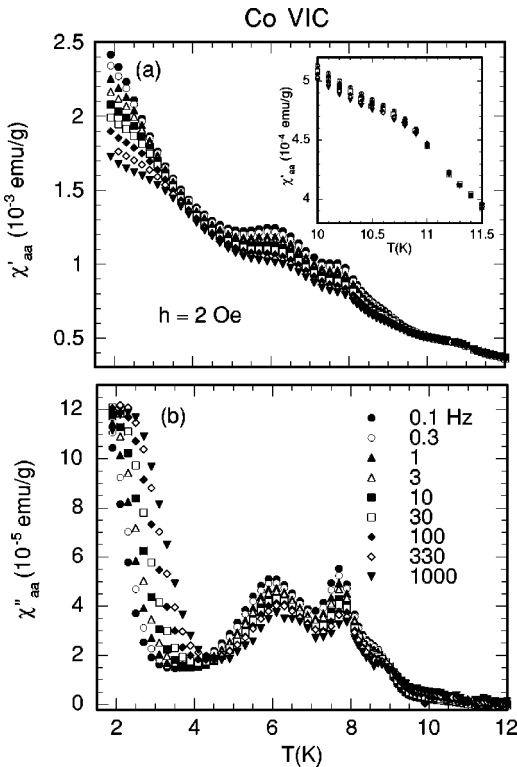


FIG. 4. T dependence of (a) χ'_{aa} and (b) χ''_{aa} for a Co VIC at various f . $h = 2$ Oe. $h \parallel a$. $H = 0$. The inset of (a) shows the detail of χ'_{aa} vs T around T_{N2} .

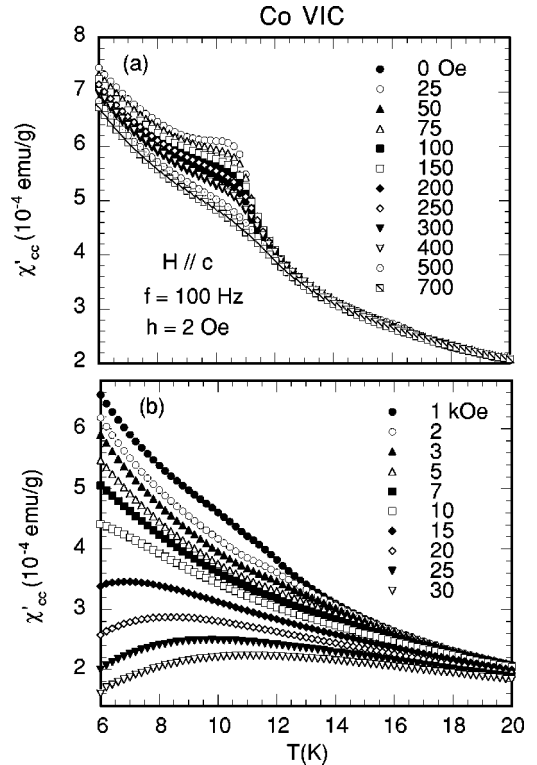


FIG. 5. (a) and (b) T dependence of χ'_{cc} for a Co VIC at various H . $H \parallel c$. $h \parallel c$. $f = 100$ Hz. $h = 2$ Oe.

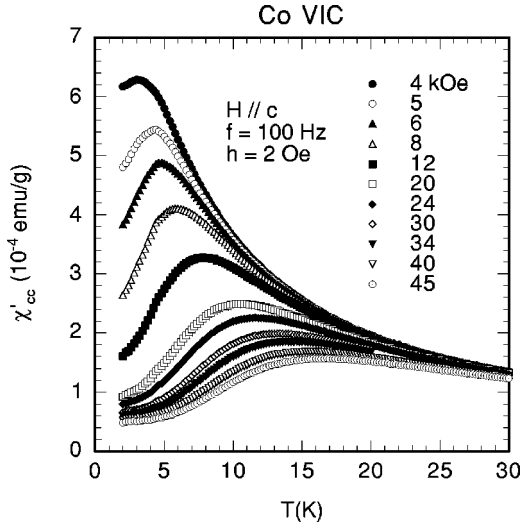


FIG. 6. T dependence of χ'_{cc} for a Co VIC at various H . $H \parallel c$. $h \parallel c$. $f = 100$ Hz. $h = 2$ Oe. These data were taken as a part of the reexamination of the H - T diagram one year later after the data of Fig. 5(b) were taken. A slight change of the data from Fig. 5(b) is seen partly because of a possible change in the quality of the sample such as a change of hydration state.

at various H along the a axis. Both peaks at T_{p1} and T_{p2} are sensitive to H and disappear above 60 Oe. The peak at T_{p1} shifts to the low T side with increasing H . A shoulder around T_{N2} remains at H up to 150 Oe. The magnetic phase diagrams for $H \parallel c$ and $H \parallel a$ will be discussed in Sec. IV B.

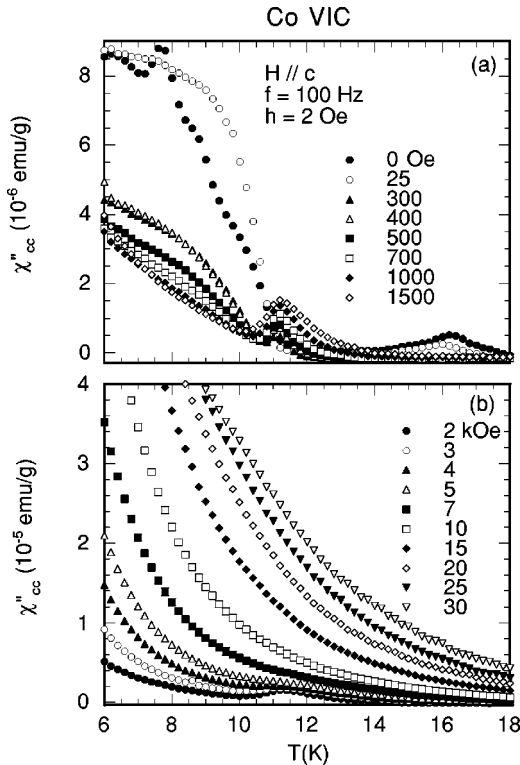


FIG. 7. (a) and (b) T dependence of χ''_{cc} for a Co VIC at various H . $H \parallel c$. $h \parallel c$. $f = 100$ Hz. $h = 2$ Oe.

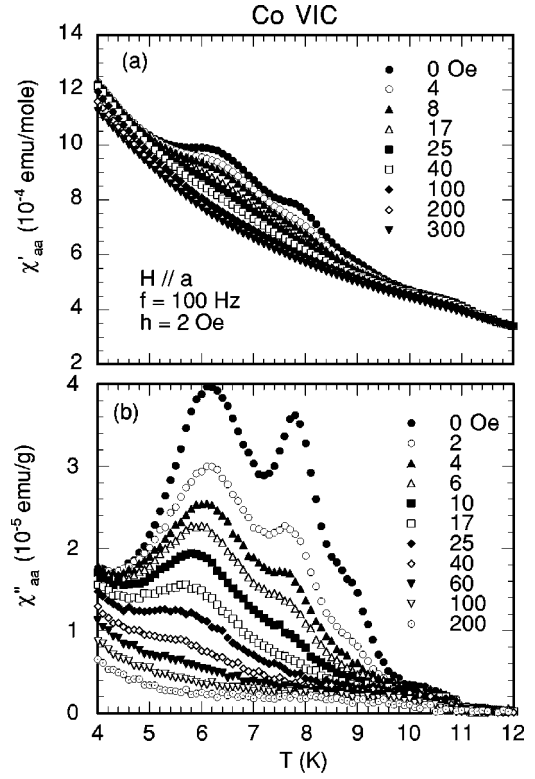


FIG. 8. T dependence of (a) χ'_{aa} and (b) χ''_{aa} for a Co VIC at various H . $H \parallel a$. $h \parallel a$. $f = 100$ Hz. $h = 2$ Oe.

IV. DISCUSSION

A. Nature of phase transitions at T_{N1} and T_{N2}

The experimental results on the phase transitions at T_{N1} and T_{N2} are summarized as follows. (i) χ''_{cc} shows a peak at T_{N1} for $H = 0$. This peak is very sensitive to the application of H along the c axis and disappears above 100 Oe. (ii) χ''_{cc} shows no peak at T_{N2} for $H = 0$. A field-induced peak appears at T just above T_{N2} for $0.3 \text{ kOe} \leq H \leq 5 \text{ kOe}$. (iii) χ'_{cc} shows a small cusp at T_{N1} and a shoulder at T_{N2} for $H = 0$. (iv) Both χ'_{aa} and χ''_{aa} show a small cusp at T_{N2} . No appreciable anomaly is observed at T_{N1} . These results indicate that the phase transitions at T_{N1} and T_{N2} are mainly owing to the orderings of the z component and the xy components of the spins, respectively. These phase transitions can be explained in terms of the model of the IHLAFT developed by Watarai and Miyashita.¹⁴ At T_{N1} the system changes from the PM phase to the FR phase (type II). The low-temperature phase below T_{N2} is characterized by the order of the xy components of spins, which grows on the order of the z component of spins that is already built in. The most favorable spin configuration is the obliquely distorted 120° structure (type III) characterized by $\varphi = 0$ and θ , where $\cos \theta = \alpha / (\alpha + 1)$. The value of α (or θ) can be estimated as follows. Miyashita and Kawamura¹¹ have discussed the values of T_{N1} and T_{N2} as a function of parameter α on the basis of the IHLAFT model. The value of T_{N1} increases proportionally with α for $\alpha > 1$, while the value of T_{N2} decreases with increasing α . The ratio $R (= T_{N1}/T_{N2})$ is approximated by $R = 2.512\alpha - 1.965$. Using our values of T_{N1} ($= 16.3$ K) and T_{N2}

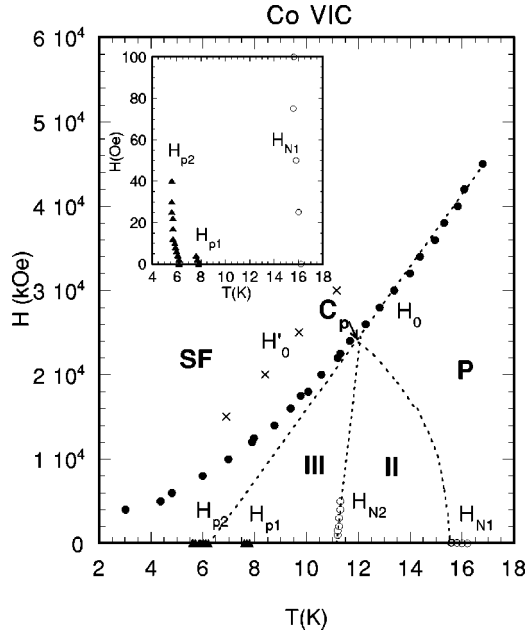


FIG. 9. Magnetic phase diagram of a Co VIC where the peak temperatures of data shown in Figs. 5–8 are plotted as a function of H . χ'_{cc} (closed circles and crosses) and χ''_{cc} (open circle) for $H\parallel c$. χ''_{aa} (closed triangles) for $H\parallel a$. Possible phase boundaries are denoted by H_0 (or H'_0), H_{N1} , H_{N2} , H_{p1} , and H_{p2} . The line H_0 is from Fig. 6 and the line H'_0 is from Fig. 5(b). The difference between the lines H_0 and H'_0 is due to the change of the quality of the sample such as the water hydration state. In spite of this fact, the line H_0 is used for the discussion of the magnetic phase diagram. Two dotted lines for possible extensions of the lines H_{N1} and H_{N2} are guides for the eye. A dotted straight line is an extrapolation of the boundary H_0 [SF-PM]. A point C_p is a multicritical point.

(=10.7 K), the parameter α is estimated as $\alpha=1.39$, or $2\theta=108.8^\circ$. In the IHLAFT model,¹⁵ both of the transitions at T_{N1} and T_{N2} belong to the universality class of a 3D XY model. The transition at T_{N1} seems to be equivalent to that of the six-state clock model since the ferrimagnetic spin arrangements can appear in six different ways over the sublattices such that $|S_A S_B S_C\rangle = |++-\rangle, |+-+\rangle, |-++\rangle, |--+\rangle, |+-\rangle$, and $|+--\rangle$. At T_{N2} , the degree of freedom of the rotation around the z axis is symmetry breaking. We find it difficult to determine the critical exponents of susceptibility at T_{N1} and T_{N2} from our results, which could be compared with the exponent predicted by Watarai and Miyashita.¹⁵

B. H - T phase diagram

Figure 9 shows the magnetic phase diagram of a Co VIC for $H\parallel c$ and $H\parallel a$. Here only the peak temperatures of χ'_{cc} , χ''_{cc} , and χ''_{aa} in Figs. 5–8 are plotted as a function of H . The magnetic phase diagram for $H\parallel c$ consists of five lines denoted by H_{N1} , H_{N2} , H_0 (or H'_0), H_{p1} , and H_{p2} . The lines H_{p1} and H_{p2} exist only for $H < 10$ Oe. The line H_{N1} exists for $0 \leq H \leq 100$ Oe and the line H_{N2} exists for $0.3 \leq H \leq 5$ kOe. The origin of the line H_0 derived from Fig. 6 is the same as that of the line H'_0 from Fig. 5(b). For comparison

these two lines are plotted in Fig. 9. The line H'_0 appears for $H \geq 15$ kOe, while the line H_0 appears for $H \geq 4$ kOe. We use the line H_0 rather than the line H'_0 for further discussion. The line H_{N1} slightly decreases with increasing T , while the line H_{N2} increases with increasing T . The line H_0 increases with increasing T at low T . It is proportional to T above 12 K. Notice that the extrapolation of this straight line to T below 12 K crosses the $H=0$ axis at T_{p2} (see Fig. 9). In spite of the lack in data at high H , the extensions of the lines H_{N1} and H_{N2} may meet at the point C_p ($T_m \approx 12$ K and $H_m \approx 25$ kOe) along dotted lines shown in Fig. 9. If this is true, our H - T phase diagram is very similar to that of an Ising-like Heisenberg antiferromagnet CsNiCl_3 (Refs. 20–23) for H along the c axis. In CsNiCl_3 , magnetic ions form a linear chain along the c axis, where the intrachain coupling is antiferromagnetic. These chains are coupled antiferromagnetically, forming a triangular lattice in the basal a - b plane. The spin easy axis is the c axis. In this sense the magnetic property of CsNiCl_3 is similar to those of a Co VIC. It may be concluded from the analogy of CsNiCl_3 that our magnetic phase diagram consists of four phases, a PM phase, a spin-flop (SF) phase, a FR (type-II) phase, and an obliquely distorted 120° structure (type III). One line of first-order transition [H_0 (SF-III)] and three lines of second-order transition [H_0 (SF-PM), H_{N1} (PM-II), and H_{N2} (II-III)] intersect at the multicritical point C_p . This type of multicritical point is predicted by an analysis of Landau-type free energy.^{22,23}

The magnetic phase diagram for $H\parallel a$ is rather different from that for $H\parallel c$. It consists of two lines denoted by H_{p1} and H_{p2} . The line H_{p1} exists for $0 \leq H \leq 4$ Oe and the line H_{p2} exists for $0 \leq H \leq 40$ Oe. The values of H_{p1} and H_{p2} decrease with increasing T . Note that no line is observed concerning the lines H_{N1} and H_{N2} . Our magnetic phase diagram is quite different from that of CsNiCl_3 where the lines H_{N1} and H_{N2} increase with increasing T .²¹ The origin for the lines H_{p1} and H_{p2} for $H\parallel a$ may be qualitatively understood as follows. Theoretically the ground-state energy of the type-III spin structure characterized by φ and θ is invariant under the rotation of φ around $\varphi=0$. This freedom of rotation may be frozen out below T_{p1} or T_{p2} , leading to a spin structure denoted by type III with $\varphi=0$. Similar behavior is observed around 3 K below T_{N2} (=4.3 K) in CsNiCl_3 from ^{133}Cs nuclear magnetic resonance,²⁴ although the heat capacity shows no anomaly around 3 K.

C. Superparamagnetic behavior

From the measurement of χ''_{cc} vs T at various f [see Fig. 4(b)], we examine the f dependence of the peak temperatures T_{p1} , T_{p2} , and T_{p3} . The values of T_{p1} and T_{p2} are almost independent of f , while the value of T_{p3} increases with increasing f . The latter implies that the characteristic relaxation time τ of the system around T_{p3} is on the order of the observation time $t_{obs} (=2\pi/\omega)$, where $\omega (=2\pi f)$ is the angular frequency of the ac field. If the relaxation of spin fluctuations is of the Debye type with a single relaxation time τ , χ''_{cc} has a peak at $\omega\tau=1$. Figure 10 shows the T dependence of τ thus obtained. The relaxation time divergingly increases

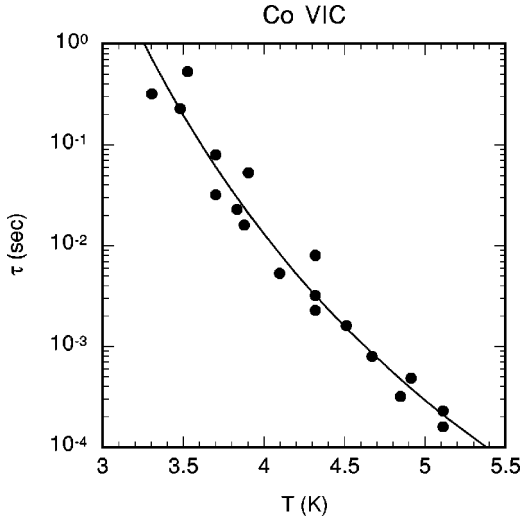


FIG. 10. T dependence of average relaxation time τ obtained from the peak temperature vs f in χ''_{cc} . The solid line denotes a least-squares fit of the data to Eq. (4) with the parameters given in the text.

with decreasing T . The most likely source of such a dramatic divergence of τ is a thermally activated relaxation used for a superparamagnet,²⁵

$$\tau = \tau_0 \exp(E_a/k_B T), \quad (4)$$

where E_a is an energy barrier separating the states and τ_0 is a microscopic limiting relaxation time. The least-squares fit of the data τ vs T as shown in Fig. 10 to Eq. (4) yields $\tau_0 = (7.3 \pm 1.0) \times 10^{-11}$ sec and $E_a/k_B = 76.0 \pm 4.1$ K for $3.3 \leq T \leq 5.1$ K. The blocking temperature T_B is defined as a temperature below which τ is larger than t_{obs} . If $t_{obs} = 1$ sec, T_B is on the order of $E_a/23k_B$ ($=3.3$ K). Below T_B the system would appear blocked in one of the states.

The possibility of spin-glass-like behaviors is ruled out for the same reasons which are described for a Ni VIC.¹⁸ The relaxation time for the droplet model²⁵ is given by $\ln(\tau/\tau_0) \propto 1/T^{1+\psi\nu}$, where $\psi\nu$ is a critical exponent. The least-squares fit of the data τ vs T in Fig. 10 to the above form yields $\tau_0 = 3.5 \times 10^{-24}$ sec and $1 + \psi\nu = 0.38 \pm 0.90$ for $3.3 \leq T \leq 5.1$ K. The value of τ_0 is too short and $\psi\nu$ becomes negative, which is inconsistent with the assumption of $\psi\nu \geq 0$. In contrast, the relaxation time for the critical slowing down model²⁶ is given by $\tau = \tau_0^*(T/T^* - 1)^{-x}$, where x is the dynamic critical exponent, T^* is the spin-freezing temperature, and τ_0^* is the characteristic relaxation time. The least-squares fit of the data τ vs T in Fig. 10 to the above form yields $x = 9.5 \pm 1.0$ and $\tau_0^* = 2.4 \times 10^{-2}$ sec. The value of x is larger than that predicted for the 3D ($\pm J$) Ising spin-glass model ($x = 7.9 \pm 1.0$).²⁷ The value of τ_0^* is unphysically large.

Thus it is concluded that a superparamagnetic behavior occurs at T_{p3} . The T dependence of τ around T_{p3} is well described by the Arrhenius law. So far the T dependence of τ is discussed only from the data of χ''_{cc} . The magnitude of χ''_{aa}

is much larger than that of χ''_{cc} at the same T below T_{p3} , indicating that the transverse fluctuations are much stronger than the longitudinal fluctuations. The absorption χ''_{aa} is strongly dependent on f and increases with decreasing T below T_{p3} . Nevertheless we cannot use the data of χ''_{aa} to determine the T dependence of τ . The Debye assumption for a single relaxation time is not satisfied for χ''_{aa} because there is no peak in χ''_{aa} at T_{p3} . The system may be a superparamagnet consisting of small magnetic clusters. Spins inside each cluster have the type-III spin structure with $\varphi=0$ and θ , where the spin planes lie in the z axis and in an arbitrary direction in the xy plane. The spin planes are different for different clusters, giving rise to the enhanced transverse spin fluctuations. Since there is no interaction between magnetic clusters, no long-range order is established.

D. Random-field effect

So far we assume that all the triangular lattice sites are uniformly occupied by Co^{2+} ions. This is not the case for our sample having a stoichiometry $X\text{Co}_u(\text{H}_2\text{O})_{6.10}$ with $u = 0.76 \pm 0.08$. The Co concentration c is given by $c = u/2$ ($0 \leq c \leq 1$).¹⁸ When Co^{2+} ions are randomly distributed on the lattice sites, the Co concentration c ($=u/2=0.38$) of our system is lower than the percolation threshold c_p^{2D} ($=0.5$) for the 2D triangular lattice,²⁸ implying no occurrence of long-range spin order in a Co VIC. This result is inconsistent with our result that the phase transitions occur at T_{N1} and T_{N2} for a Co VIC. Co^{2+} ions may not be randomly distributed on the lattice sites over the whole system. One possibility is that small islands are formed inside the Co layers. In each island Co^{2+} ions may be uniformly located on the triangular lattice ($c=1$), or randomly distributed on the lattice sites with a concentration c which is much higher than c_p^{2D} . For the former case, the system is essentially the same as the ideal case ($c=1$) with a finite-size effect. For the latter case, the system is a diluted Ising-like antiferromagnet on the triangular lattice. The application of a uniform magnetic field on such 3D diluted Ising-like antiferromagnets generates an effective random field which couples to the antiferromagnetic order parameter, producing a realization of the random-field (RF) model.²⁹ What is the evidence for such a RF effect? As shown in the insets of Figs. 2(a) and 2(b), the irreversible effect of susceptibility shows two steplike changes around T_{N1} and T_{N2} in $\delta\chi_c$ and $\delta\chi_a$. The magnitude of $\delta\chi_c$ is larger than that of $\delta\chi_a$ at the same T above 9 K. These anomalies may be related to the RF effect. The ZFC measurement shows a sharp transition to a long-range ordered state, while the FC procedure causes the system to lose equilibrium and enter a metastable, frozen domain state without a long-range order. Similar behavior is observed in reentrant spin-glass systems $\text{Ni}_c\text{Mg}_{1-c}(\text{OH})_2$ ($c=0.8$) (Ref. 30) and $\text{Fe}_c\text{Mn}_{1-c}\text{TiO}_3$ ($c=0.6$).³¹ The irreversible effect of susceptibility exhibits a crossover from a weak irreversibility just below the Néel temperature $T_N(H)$ to a strong irreversibility at a reentrant spin-glass (RSG) transition temperature $T_{RSG}(H)$. Additional possible evidence for the RF effect is that the magnitude of χ''_{cc} becomes large with increasing H

for $H \geq 7$ kOe, as shown in Fig. 7(b). Numerical calculations³²⁻³⁴ based on the molecular-field theory for a 3D diluted Ising antiferromagnet suggest that a region of antiferromagnetic long-range order and a region of glassy state exist in the H - T plane. The glassy phase remains restricted to large H , where the strength of the random field varies with H . Enhancement of χ''_{cc} at large H may be related to the RF-induced glassy phase. A detailed discussion will be given elsewhere.

E. Superexchange interaction mechanism

The intraplanar exchange interaction is antiferromagnetic in a Co VIC and ferromagnetic in a Ni VIC. What is the cause of this difference? In a M VIC ($M=\text{Co, Ni}$), each M^{2+} ion is located at the m_1 sites between triangular groups of surface oxygens forming the bases of the SiO_2 and AlO_4 tetrahedrons.¹⁸ The O^{2-} ions form a 2D *kagomé*-like lattice. The magnetic M^{2+} ion at the m_1 sites is surrounded by nearest-neighbor O^{2-} ions in an approximately octahedral cubic crystal environment with a small trigonal distortion (along the c axis). These local structures are similar to those of pristine $M\text{Cl}_2$ where M is surrounded by six Cl^- ions. As has been already pointed out by Zhou *et al.*,¹⁷ the intraplanar exchange interaction between M^{2+} ions is probably caused by the so-called superexchange, which is due to the overlap of the localized orbitals of M^{2+} ions with those of those of O^{2-} ions.³⁵ An empirical rule (Goodenough-Kanamori^{36,37}) is well established for determining the sign of the superexchange interaction (ferromagnetic or antiferromagnetic) from the symmetry relation between the occupied d orbitals ($d\epsilon$ and $d\gamma$) for the M^{2+} ion and occupied p orbitals (p_σ and p_π) for the O^{2-} ion. There are two types of superexchange depending on the angle ϕ between two $M^{2+}\text{O}^{2-}$ bonds in the $M^{2+}\text{-O-M}^{2+}$ link: $\phi=180^\circ$ and 90° .

Here we consider the origin of the intraplanar interaction in a M VIC by applying the Goodenough-Kanamori rule with $\phi=90^\circ$. The electronic configuration of the lowest orbital state of the M^{2+} ions which is subject to an octahedral cubic field is $(d\epsilon^6)d\gamma^2$ for a Ni^{2+} ion and $(d\epsilon^4)d\epsilon^1d\gamma^2$ for a Co^{2+} ion,³⁷ where orbital states in parentheses indicate paired electrons. In the Co^{2+} ion the Coulomb interaction between the electrons causes a configurational mixing. The origin of ferromagnetic interaction between Ni^{2+} ions in a Ni VIC is similar to that of pristine NiCl_2 .³⁷ The O^{2-} ion has two electrons with spins up and down. There is some probability that less than one electron is transferred from the p_σ orbital of O^{2-} to the $d\gamma$ orbital of Ni^{2+} because the p_σ orbital forms a partially covalent bond with the $d\gamma$ orbital. The electron left behind on the O^{2-} ion has its spin parallel to the spin of the Ni^{2+} ion. Since the p_σ orbital of the O^{2-} ion is orthogonal to the $d\gamma'$ orbital of the other Ni^{2+} ion, the direct exchange interaction between the remaining unpaired spin on the O^{2-} ion and the Ni^{2+} spins is ferromagnetic. This leads to the ferromagnetic exchange interaction between Ni^{2+} spins.

What is the origin of the antiferromagnetic intraplanar interaction between Co^{2+} ions in a Co VIC? There are two possibilities giving rise to the antiferromagnetic intraplanar

interaction. There is one probability that less than one electron is transferred from the p_π orbital of the O^{2-} ion to the $d\epsilon$ orbital of the Co^{2+} ion because the p_π orbital forms a partially covalent bond with the $d\epsilon$ orbital. The electron left behind on the O^{2-} ion has its spin parallel to the spin of the Co^{2+} ion. The p_π orbital of the O^{2-} ion is antiferromagnetically coupled to the $d\gamma'$ orbital of the other Co^{2+} ion, leading to the antiferromagnetic intraplanar exchange interaction between Co^{2+} spins. There is another possibility that less than one electron is transferred from the p_σ orbital of the O^{2-} ion to the $d\gamma$ orbital of the Co^{2+} ion because the p_σ orbital forms a partially covalent bond with the $d\gamma$ orbital. The electron left behind on the O^{2-} ion has its spin parallel to the spin of the Co^{2+} ion. The p_σ orbital of the O^{2-} ion is antiferromagnetically coupled to the $d\epsilon'$ orbital of the other Co^{2+} ion, leading to the antiferromagnetic intraplanar exchange interaction between Co^{2+} spins. The latter antiferromagnetic interaction is stronger than the former one because the $d\epsilon$ - p_π bond is weaker than the $d\gamma$ - p_σ bond due to a smaller overlap of wave functions.³⁷

Finally we discuss the effective spin Hamiltonians of a Ni VIC and a Co VIC. The lowest orbital state of the free Ni^{2+} ion (derived from the electronic configuration $3d^8$) is 3F_4 . In a cubic crystal field, the 3F_4 state is split into two orbital triplets (3T_1 and 3T_2) and one orbital singlet (3A_2) as a lowest level.³⁸ Since the orbital angular momentum for the 3A_2 state is fully quenched, no additional splitting is done by the spin-orbit interaction and trigonal crystal field. The ground state is threefold spin degenerate, leading to the effective spin Hamiltonian with $S=1$. In contrast, the lowest orbital state of the free Co^{2+} ion (derived from the electronic configuration $3d^7$) is ${}^4F_{9/2}$. In a cubic crystal field, the ${}^4F_{9/2}$ state is split into two orbital triplets (4T_1 and 4T_2) and one orbital singlet (4A_2) with the orbital triplet (4T_1) lowest.³⁸ The ground orbital triplet is split by the spin-orbit coupling and trigonal field. The lowest level is a Kramers doublet, leading to the effective spin Hamiltonian with a fictitious spin $S=1/2$.

V. CONCLUSION

A Co VIC with a 2-WLHS behaves magnetically as an Ising-like Heisenberg antiferromagnet on the triangular lattice. This compound undergoes two magnetic phase transitions T_{N1} ($=16.3$ K) and T_{N2} ($=10.7$ K). At T_{N1} the longitudinal (c -axis) spin component orders and a ferrimagnetic (type-II) phase is realized for $T_{N2} < T < T_{N1}$. At T_{N2} the transverse component orders and an obliquely distorted 120° spin structure (type III) is stabilized for $T < T_{N2}$. The magnetic phase diagram for $H \parallel c$ consists of four phases (II, III, PM, and SF) whose boundaries would meet at a multicritical point ($T_m \approx 12$ K, $H_m \approx 25$ kOe). The system also shows magnetic anomalies at T_{p1} ($=7.7$ K), T_{p2} ($=5.9$ K), and T_{p3} (≈ 3 K). The anomalies at T_{p1} or T_{p2} may be related to the freezing out of the freedom of rotation around an axis perpendicular to the spin plane. The spin-relaxation time diverges at T_{p3} according to the Arrhenius law, suggesting that the system may be a superparamagnet consisting of small magnetic clusters with the type-III spin structures hav-

ing different spin planes. Magnetic neutron scattering on a Co VIC with all hydrogen atoms replaced by deuterium and magnetic heat capacity would be required for the further understanding of the nature of successive phase transitions and the magnetic phase diagram.

ACKNOWLEDGMENT

The work at the State University of New York (SUNY) at Binghamton was partially supported by the Research Foundation of SUNY-Binghamton (Contract No. 9522A).

*Email address: itsuko@binghamton.edu

- ¹M. Mekata, J. Phys. Soc. Jpn. **42**, 76 (1977).
- ²M. Mekata and K. Adachi, J. Phys. Soc. Jpn. **44**, 806 (1978).
- ³H. Yoshizawa and K. Hirakawa, J. Phys. Soc. Jpn. **46**, 448 (1979).
- ⁴M. Mekata, J. Magn. Magn. Mater. **90 & 91**, 247 (1990).
- ⁵S. Fujiki, K. Shutoh, and S. Katsura, J. Phys. Soc. Jpn. **53**, 1371 (1984).
- ⁶H. Takayama, K. Matsumoto, H. Kawahara, and K. Wada, J. Phys. Soc. Jpn. **52**, 2888 (1983).
- ⁷S. Miyashita, H. Kitatani, and Y. Kanada, J. Phys. Soc. Jpn. **60**, 1523 (1991).
- ⁸S. Mitsuda, H. Yoshizawa, N. Yaguchi, and M. Mekata, J. Phys. Soc. Jpn. **60**, 1885 (1991).
- ⁹M. Mekata, N. Yaguchi, T. Takagi, T. Sugino, S. Mitsuda, H. Yoshizawa, N. Hosoito, and T. Shinjo, J. Phys. Soc. Jpn. **62**, 4474 (1993).
- ¹⁰K. Takeda, K. Miyake, M. Hitaka, T. Kawae, N. Yaguchi, and M. Mekata, J. Phys. Soc. Jpn. **63**, 2017 (1994).
- ¹¹S. Miyashita and H. Kawamura, J. Phys. Soc. Jpn. **54**, 3385 (1985).
- ¹²S. Miyashita, J. Phys. Soc. Jpn. **55**, 227 (1986).
- ¹³S. Miyashita, J. Phys. Soc. Jpn. **55**, 3605 (1986).
- ¹⁴S. Watarai and S. Miyashita, J. Phys. Soc. Jpn. **63**, 1916 (1994).
- ¹⁵S. Watarai and S. Miyashita, J. Phys. Soc. Jpn. **67**, 816 (1998).
- ¹⁶M. Suzuki, M. Yeh, C.R. Burr, M.S. Whittingham, K. Koga, and H. Nishihara, Phys. Rev. B **40**, 11 229 (1989), and references therein.
- ¹⁷P. Zhou, J. Amarasekera, S.A. Solin, S.D. Mahanti, and T.J. Pinnavaia, Phys. Rev. B **47**, 16 486 (1993).
- ¹⁸M. Suzuki, I.S. Suzuki, N. Wada, and M.S. Whittingham, Phys. Rev. B **64**, 104418 (2001).
- ¹⁹N. Achiwa, J. Phys. Soc. Jpn. **27**, 561 (1969).
- ²⁰P.B. Johnson, J.A. Rayne, and S.A. Friedberg, J. Appl. Phys. **50**, 1853 (1979).
- ²¹Y. Trudeau, M.L. Plumer, M. Poirier, and A. Caillé, Phys. Rev. B **48**, 12 805 (1993).
- ²²H. Kawamura, A. Caillé, and M.L. Plumer, Phys. Rev. B **41**, 4416 (1990).
- ²³M.L. Plumer, A. Caillé, and H. Kawamura, Phys. Rev. B **44**, 4461 (1991).
- ²⁴S. Maegawa, T. Goto, and Y. Ajiro, J. Phys. Soc. Jpn. **57**, 1402 (1988).
- ²⁵D.S. Fisher and D.A. Huse, Phys. Rev. B **36**, 8937 (1987).
- ²⁶J.A. Mydosh, *Spin Glasses: An Experimental Introduction* (Taylor & Francis, London, 1993).
- ²⁷A.T. Ogielski, Phys. Rev. B **32**, 7384 (1985).
- ²⁸R.B. Stinchcombe, in *Phase Transitions and Critical Phenomena*, edited by C. Domb and J.L. Lebowitz (Academic Press, London, 1983), Vol. 7, p. 151.
- ²⁹D.P. Belanger, in *Spin Glasses and Random Fields*, edited by A.P. Young (World Scientific, Singapore, 1998), p. 251.
- ³⁰M. Suzuki, I.S. Suzuki, and T. Enoki, (unpublished).
- ³¹H. Yoshizawa, H. Mori, H. Kawano, H. Aruga Katori, S. Mitsuda, and A. Ito, J. Phys. Soc. Jpn. **63**, 3145 (1994).
- ³²C. Ro, G.S. Grest, C.M. Soukoulis, and K. Levin, Phys. Rev. B **31**, 1682 (1985).
- ³³J.R.L. de Almeida and R. Bruinsma, Phys. Rev. B **35**, 7267 (1987).
- ³⁴G.S. Grest, C.M. Soukoulis, and K. Levin, Phys. Rev. B **33**, 7659 (1986).
- ³⁵P.W. Anderson, in *Solid State Physics*, edited by F. Seitz and D. Turnbull (Academic Press, New York, 1963), Vol. 14, p. 99.
- ³⁶J.B. Goodenough, *Magnetism and the Chemical Bond* (Interscience, New York, 1963).
- ³⁷J. Kanamori, J. Phys. Chem. Solids **10**, 87 (1959).
- ³⁸M.E. Lines, Phys. Rev. **131**, 546 (1963).